transition to relaxation oscillations.

To end this case study, we report the existence of a different type of MMO not found by Koper; it is shown in Figure 22. The MMO has SAOs both near the maximum and the minimum of the LAO. Hence, this MMO passes near folded nodes $n_{\pm}^{a}$ on both fold curves. The parameter region where this occurs is quite small, so that it is difficult to locate such an MMO using simulation; it is the region in Figure 16 near $k = -2$ that can only be seen in the enlargement in panel (b). We found the MMO by selecting parameters $k = -2.1$ and $\lambda = -0.063$ in this region and choose $\varepsilon_1 = 0.01$ rather small; a more detailed study of the range of parameters for which such MMOs with two SAO epochs remains future work.

5. MMOs in a reduced Hodgkin–Huxley system. As the next case study we consider a three-dimensional reduced version of the famous Hodgkin–Huxley equations [102] that describe the generation of action potentials in the squid giant axon; see [115, 196] for the derivation and also [43], where the same example was used. The reduced model only describes the dynamics for voltage (V), the activation of the potassium channels (n) and the inactivation of the sodium channels (h); the activation of the sodium channels (m) is very fast and it reaches its equilibrum state $m = m_\infty(V)$ (almost) instantaneously which can be justified mathematically by a center-manifold reduction [196]. The evolution of the gates n and h is considered slow while the evolution of the voltage V is considered fast. To justify this time-scale separation, we nondimensionalize the Hodgkin–Huxley equations by introducing a dimensionless voltage variable $v = V/k_v$ and a dimensionless time $\tau = t/k_t$ where $k_v = 100$ mV is a reference voltage scale and $k_t = 1$ ms is a fast reference time scale; this gives

$$\left\{\begin{array}{rcll} \varepsilon\dot{v} &=& f(v,h,n) &:= \bar{I} - m_\infty^3(v)\,h\,(v-\bar{E}_{\rm Na}) \\ & & & \quad -\bar{g}_k\,n^4\,(v-\bar{E}_{\rm K}) - \bar{g}_l\,(v-\bar{E}_{\rm L}), \\ \dot{h} &=& g_1(v,h) &:= \dfrac{k_t}{\tau_h}\,\dfrac{(h_\infty(v)-h)}{t_h(v)}, \\ \dot{n} &=& g_2(v,n) &:= \dfrac{k_t}{\tau_n}\,\dfrac{(n_\infty(v)-n)}{t_n(v)}, \end{array}\right. \tag{5.1}$$

with dimensionless parameters $\bar{E}_x = E_x/k_v$, $\bar{g}_x = g_x/g_{\rm Na}$, with $x \in \{m,\ n,\ h\}$, $\bar{I} = I/(k_v g_{\rm Na})$ and $\varepsilon = C/(k_t g_{\rm Na}) =: \tau_v/k_t$. The original Hodgkin–Huxley parameter values are given in Table 5.1. Thus, $\varepsilon = \frac{1}{120} \approx 0.01 \ll 1$ and system (5.1) represents a singularly perturbed system with v as a fast variable and (n,h) as slow variables. The functions $x_\infty(v)$ and $t_x(v)$, with $x \in \{m,\ n,\ h\}$, describe the (dimensionless) steady-state values and time constants of the gating variables, respectively; they are given by

$$x_\infty(v) = \frac{\alpha_x(v)}{\alpha_x(v)+\beta_x(v)} \quad \text{and} \quad t_x(v) = \frac{1}{\alpha_x(v)+\beta_x(v)},$$

with

$$\begin{array}{rclrcl} \alpha_m(v) &=& \frac{(k_v v+40)/10}{1-\exp(-(k_v v+40)/10)}, & \beta_m(v) &=& 4\exp(-(k_v v+65)/18), \\ \alpha_h(v) &=& 0.07\exp(-(k_v v+65)/20), & \beta_h(v) &=& \frac{1}{1+\exp(-(k_v v+35)/10)}, \\ \alpha_n(v) &=& \frac{(k_v v+55)/100}{1-\exp(-(k_v v+55)/10)}, & \beta_n(v) &=& 0.125\exp(-(k_v v+65)/80). \end{array}$$

The orginal Hodgkin–Huxley equations with scaling parameters $\tau_h = \tau_n = \tau_m = 1$ shows no MMOs [102], but if $\tau_h > \tau_{h,e} > 1$ or $\tau_n > \tau_{n,e} > 1$ are beyond certain threshold

g_{Na}	g_k	g_l	E_{Na}	E_{K}	E_{L}	τ_h	τ_n	C
120.0	36.0	0.3	50.0	-77.0	-54.4	1.0	1.0	1.0

TABLE 5.1
Original parameter values of the Hodgkin–Huxley equations (5.1).

values then MMOs are observed [43, 196, 197]. Here, we focus on a specific case with $\tau_h = 6.0$, $\tau_n = 1.0$ and $C = 1.2$ (so that $\varepsilon = 0.01$). We use the applied current I (in units of $\mu\mathrm{A}/\mathrm{cm}^2$) of the original Hodgkin–Huxley equations, that is, the rescaled $\bar{I}$ in (5.1), as the only free parameter. Furthermore, in order to facilitate comparison with other studies, we represent output in terms of the non-rescaled voltage $V = 100\,v$, which is in units of mV.

From a mathematical point of view, the MMOs are generated due to the presence of a (subcritical) singular Hopf bifurcation at $I = I_H \approx 8.359$ and a folded node in the singular limit $\varepsilon = 0$. The critical manifold of (5.1) is defined by,

$$n^4(v,h) = \frac{\bar{I} - m_\infty(v)^3\, h\,(v - \bar{E}_{\mathrm{Na}}) - \bar{g}_L\,(v - \bar{E}_l)}{\bar{g}_k\,(v - \bar{E}_k)},$$

which is a cubic-shaped surface $S = S^{a,-} \cup F_- \cup S^r \cup F_+ \cup S^{a,+}$ for physiologically relevant values of I. The outer sheets $S^{a,\pm}$ are stable, the middle sheet S^r is unstable, and $F_\pm$ denote fold curves [196]. The desingularized reduced system on this manifold is given by

$$\left\{ \begin{array}{rcl} \dot{v} &=& \left(\frac{\partial}{\partial h} f\right) g_1 \quad + \quad \left(\frac{\partial}{\partial n} f\right) g_2, \\ \dot{h} &=& -\left(\frac{\partial}{\partial v} f\right) g_1. \end{array} \right.$$

A phase-plane analysis of the desingularized reduced flow in the physiologically relevant range shows that there exists a folded node singularity on F_- for $I > I_{FSN} \approx 4.83$. Furthermore, it can be shown that the global-return mechanism projects into the funnel region for $I < I_r \approx 15.6$; see [196, 197]. Hence, the folded node theory predicts the existence of stable MMOs for a range of I-values that converges to $I_{FSN} < I < I_r$ in the singular limit as $\varepsilon \to 0$.

Figure 23(a) shows the folded node singularity for $I = 12$, where it lies approximately at $(v, h, n) = (-0.593, 0.298, 0.407)$, in projection onto the (n, V)-plane. The two black curves are the strong singular canard $\tilde{\gamma}_s$ and the primary weak canard γ_w that pass through the folded node. The other two curves are maximal secondary canards ξ_5 and ξ_6 that were found as intersections of extended slow manifolds computed near the folded node; see also Section 8 and [43, Figure 6]. Their projections onto the (h, V)-plane, which illustrate the oscillating nature of ξ_5 and ξ_6, are shown in Figure 23(b). Notice that the final oscillations of the primary weak canard γ_w in Figure 23(a) show the distinct characteristics of saddle-focus-induced SAOs. Indeed, a saddle-focus equilibrium $q \approx (-0.589, 0.379, 0.414)$ exists relatively close to the folded node, due to the singular Hopf bifurcation at $I_H \approx 8.359$. Decreasing I from $I = 12$ toward $I = I_H$ causes q to move closer to the folded node and the mix of folded node induced SAOs and saddle-focus induced SAOs will be more pronounced; compare with Figure 21(c).

The equilibrium q for $I = 12$ persists when I is varied. A partial bifurcation diagram is shown in Figure 24(a), where we plot the maximum of V versus I. Similar to the analysis in [43], a unique equilibrium exists for all I and it is stable for $I < I_H$ and, approximately, $I > 270.772$. The (singular) Hopf bifurcation (labeled H) at I_H gives rise to a family of saddle-type periodic orbits. This family of periodic orbits undergoes three fold bifurcations (SL) at $I \approx 6.839$, $I \approx 27.417$ and $I = I_{SL} \approx 14.860$, after which both non-trivial Floquet

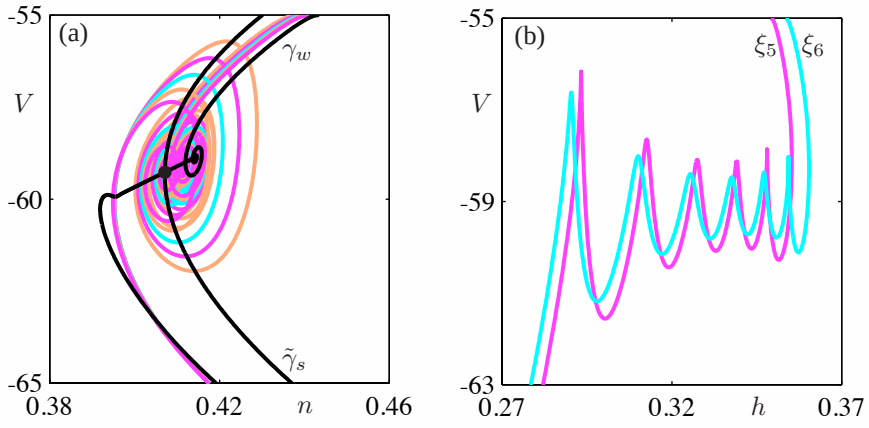

FIG. 23. *Maximal secondary canard orbits ξ_5 and ξ_6 of the three-dimensional reduced Hodgkin–Huxley equations* (5.1) *with $\tau_h = 6.0$, $\tau_n = 1.0$, $C = 1.2$ and $I = 12$. Panel (a) shows the two canard orbits in projection onto the (n, V)-plane; also shown are the strong singular canard $\tilde{\gamma}_s$ and the weak primary canard γ_w. The projection of ξ_5 and ξ_6 onto the (h, V)-plane in panel (b) shows that they make five and six oscillations, respectively.*

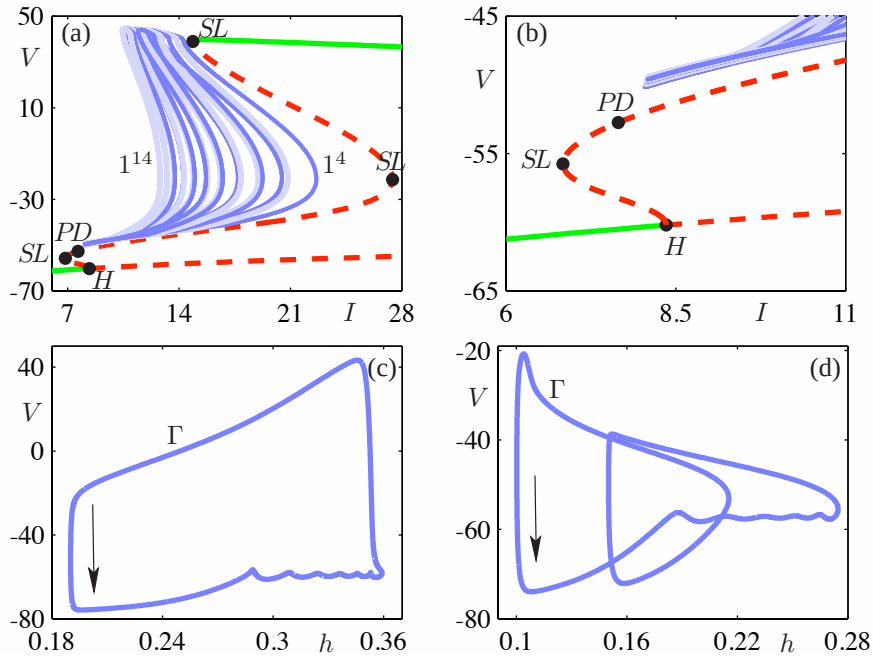

FIG. 24. *MMO periodic orbits of the three-dimensional reduced Hodgkin–Huxley equations* (5.1) *with $\tau_h = 6.0$, $\tau_n = 1.0$ and $C = 1.2$. Panel (a) shows a bifurcation diagram where the maximal V-value is plotted versus the applied current I. Isolas of MMO periodic orbits exist over a range of I bounded by a period-doubling bifurcation* PD *and a saddle-node of limit cycle bifurcation* SL. *The isolas are colored in alternating light and dark blue. Panel (b) shows an enlargement near the Hopf bifurcation. All isolas shown have a fold bifurcation for $I_{SL} \approx 8.087$. The periodic orbit Γ shown in panel (c) is the stable MMO for $I = 12$; panel (d) shows Γ when it has a maximal V-value of -20 mV.*

multipliers are less than 1 in modulus and the associated stable periodic orbits correspond to tonic spiking. Figure 24(a) shows that the first SL is quickly followed by a period-doubling bifurcation (PD) at $I \approx 7.651$, where one of the Floquet multipliers, which are both unstable after this first SL, passes through -1. Hence, the periodic orbits after PD are non-orientable and of saddle type. Note that a second PD (not shown in Figure 24(a)) must take place before the second SL.

MMOs exist as isolated families of periodic orbits for a range of I; Figure 24(a) shows eleven of these isolas colored in alternating light and dark blue. All periodic orbits on a single isola have the same number of oscillations. Each isola contains a short plateau with large maximal V near $V = 40$ mV where the associated MMOs are stable and have signatures 1^s. For our specific choice $\varepsilon = 0.01$, we found that the stable MMO interval appears to be bounded by I_H on the left and by I_{SL} on the right, that is, $8.359 < I < 14.860$. Recall that the theory based on the singular limit as $\varepsilon \to 0$ predicts the existence of stable MMO periodic orbits with signatures 1^s for $4.83 \approx I_{FSN} < I < I_r \approx 15.6$; the match is surprisingly good, even though ε is relatively large. As $I \downarrow I_H$, the number s in the stable 1^s MMO signatures approaches infinity, since a homoclinic orbit through the Hopf singularity is formed; see also [43]. Furthermore, there exist stable MMO signatures with more complicated signatures $1^{s_1}1^{s_2}\cdots$; see [197]. The MMO periodic orbits go through several bifurcations along the isolas (mostly period-doubling and/or saddle-node of limit cycle bifurcations); compare also Figure 19 for the Koper model in Section 4. The maximal V-value indicates the amplitude of the largest of the oscillations of the respective MMO periodic orbit. Note the folded structure of the isolas for $V = V_{F_+} \approx -20$ mV which is approximately the repolarization threshold value for action potentials. This value also corresponds to the V-value of the upper fold curve F_+, at which a trajectory jumps back. For MMOs on a plateau, the LAOs correspond to a full action potential, while the s SAOs that follow are subthreshold oscillations.

Figure 24(b) shows an enlargement of how the isolas of MMO periodic orbits accumulate near the Hopf bifurcation, which is the region where theory predicts a signature 1^s, that is, an MMO with one large excursions and s SAOs. This is organised by how the global-return mechanism projects onto the critical manifold S as I varies. If the return projects onto a secondary canard then part of the periodic orbit follows the secondary canards onto the unstable branch $S_{r,\varepsilon}$ of the slow manifold. However, only canard periodic orbits that reach the region of the upper fold curve F_+ are maximal secondary canards. Hence, the corresponding family of secondary canards can be split into two groups: we call the secondary canards with maximum $V < V_{F_+}$ *jump-back* canards and those with maximum $V > V_{F_+}$ *jump-away* canards. This is an important distinction in this application, because the jump-away canards will create action potentials, the jump-back canards will not.

We illustrate the canards along one of the isolas in Figures 24(a) and (b). The stable MMO periodic orbit Γ that exists on the plateau for $I = 12$ is shown in Figure 24(c); its signature is 1^6 and it lies on the isola that corresponds to periodic orbits with a total of seven oscillations. Note that the large excursion of Γ is above threshold. The six SAOs of Γ are due to the fact that the global return lands on the rotational sector bounded by the maximal secondary canards ξ_5 and ξ_6 for $I = 12$ (not shown); compare Figures 23(b). When the periodic orbit Γ is continued in the direction of increasing I, the maximal V-value decreases and the LAO changes from an action potential to a sub-threshold oscillation. Figure 24(d) shows Γ (which is now unstable) when its maximal V-value is approximately -20 mV. Observe that Γ still has a total of seven oscillations, but now two of them have a fast segment. These fast segments are jump-back canards. More precisely, the periodic orbit Γ consists of a segment of a jump-back canard of the ξ_6 canard family that connects to a segment of a jump-back canard of the strong canard family, which in turn connects to the former segment, hence, closing the

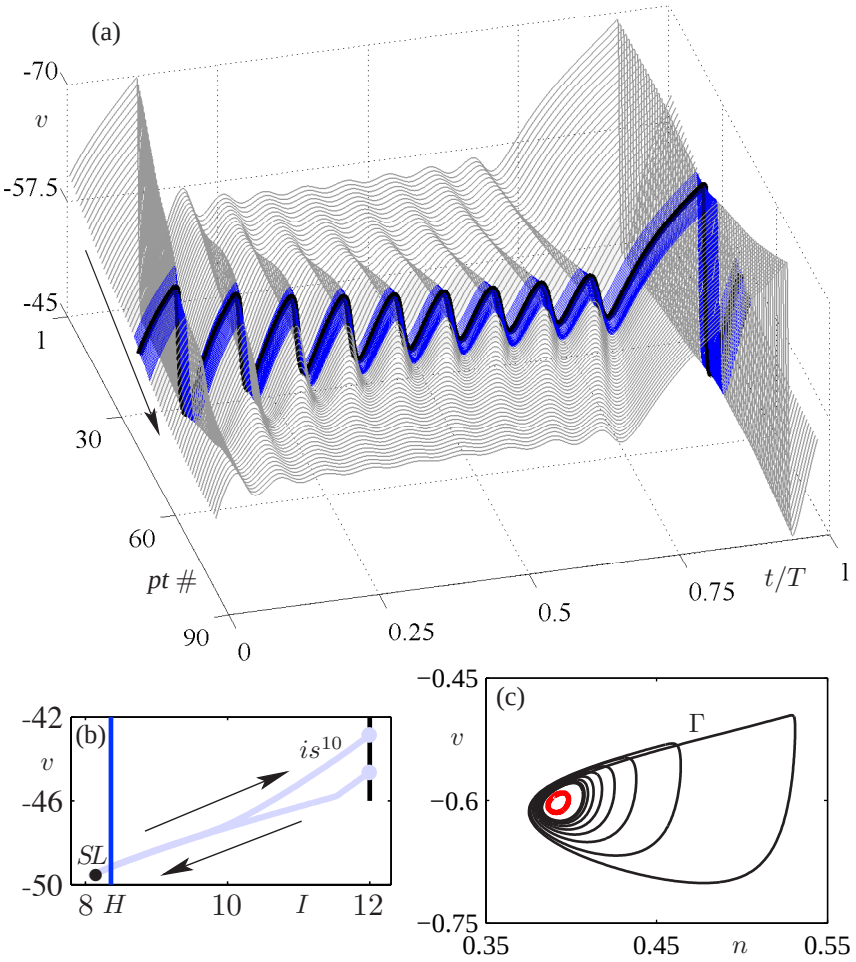

FIG. 25. *Continuation of a family of periodic orbits that consist of ten oscillations. The continuation starts and ends at $I = 12$ with a fold at $I \approx 8.087$. Panel (a) shows a three-dimensional "waterfall diagram" visualization of the time series of V for 90 computed periodic orbits along this part of the isola; the boldface periodic orbit lies at the fold point. The orbits in blue correspond to the part of isola in between the fold point and the I-value that corresponds to the Hopf bifurcation, that is, $I_H \approx 8.359$. Panel (b) shows the maximal V-value along the branch in the (I, V)-plane, where the arrows indicate the direction of the continuation. Panel (c) shows the periodic orbit at the fold together with a coexisting small periodic orbit in projection onto the (n, v)-plane.*

loop. One could classify Γ in Figure 24(d) as an MMO with signature 2^5, because only five of its oscillations have really small amplitude due to the passage near the folded node, while there are two clearly distinguishable larger oscillations with fast segments due to jump-back canards. However, none of these larger canard oscillations of Γ are full action potentials, meaning that all oscillations are classified as SAOs in this application context.

Figure 25 illustrates the characteristics of the periodic orbits along the lower parts of the isolas in Figure 24(a), where they are very close to the branch of saddle periodic orbits bifurcating from the Hopf bifurcation. More specifically, Figure 25(a) shows a "waterfall diagram" representation of the time series of 90 periodic orbits along the lower part, for $I \leq 12$, of the isola along which one finds a total of ten oscillations. This part of the branch is

TABLE 6.1
Parameter values used in the four-dimensional Olsen model (6.1)

k_1	k_2	k_3	k_4	k_5	k_6	k_7	k_{-7}	k_8	α
0.28	250	0.035	20	5.35	0	0.8	0.1	0.825	1

shown in Figure 25(b). The fold point for this isola is at $I = I_{SL} \approx 8.087$, and the associated periodic orbit is drawn in boldface in Figure 25(a). The periodic orbits on the part of the branch for $I_{SL} \leq I \leq I_H$ are highlighted in blue. The periodic orbits along this part of the isola are quite different from the MMOs one finds near the plateaux of the isolas; Namely, they consist of a mix of SAOs and jump-back canards, ten in total. Figure 25(c) shows the projection of the periodic orbit at the fold onto the (n, V)-plane; also shown is the coexisting small periodic orbit that lies on the branch emanating from the Hopf bifurcation. This figure suggests that the periodic orbit at the fold is approaching a homoclinic cycle of the small periodic orbit.

6. MMOs in Olsen's four-dimensional model of the PO reaction. Many applications do not lead to models that have a clear split into slow and fast time scales. Often some assumptions to that extent can be made, but most variables will be slow in certain regions of phase space and fast in others. The following case study illustrates how the geometrical ideas from slow-fast systems can be used in such a context. We study a four-dimensional model of the peroxidase-oxidase (PO) biochemical reaction that was introduced by Olsen and collaborators [37, 172]; see also [42], where this same example was used. The Olsen model describes dynamics of the concentrations of two substrates (O_2 and $NADH$) and two free radicals, denoted A, B, X and Y, respectively; it is given by the differential equations

$$\begin{cases} A' &= -k_3ABY + k_7 - k_{-7}A, \\ B' &= \alpha(-k_3ABY - k_1BX + k_8), \\ X' &= k_1BX - 2k_2X^2 + 3k_3ABY - k_4X + k_6, \\ Y' &= -k_3ABY + 2k_2X^2 - k_5Y. \end{cases} \tag{6.1}$$

Note that α is an artificial time-scale parameter that we introduced for the purpose of this case study; $\alpha = 1$ in [37, 172]. The other parameters are reaction rates and we chose their values as given in Table 6.1, such that the periodic orbits that exist for these parameter values are representative for the Olsen model (6.1). We focus our study on a stable MMO periodic orbit, denoted Γ; its time series of the variable A is shown in Figure 26(b). We observe that Γ has signature 1^s, and we estimate that s is about 15. Below, we show that the SAOs of this example occur during passage through a dynamic Hopf bifurcation, and we analyze the global return mechanism of this trajectory.

6.1. Bifurcations of the fast subsystem. There is no clear split between the different time scales in the Olsen model (6.1), but it is known that B evolves on a slower time scale than the other variables [153]. Hence, it makes sense to consider the fast subsystem obtained by setting $\alpha = 0$, that is, $B' = 0$ and B acts as a parameter in (6.1). The bifurcation diagram is shown in projection onto the (A, B)-plane in Figure 26(a), which is invariant because $k_6 = 0$; see Table (6.1). There are two branches of equilibria that intersect at a transcritical bifurcation T for $B = k_4/k_1 \approx 71.426$; solid lines indicate stable and dashed lines unstable equilibria. The equilibria that are colored black in Figure 26(a) are physically relevant because they have non-negative values of X and Y; for grey equilibria, on the other hand, X or Y is negative. One branch is the black horizontal line at $A = 8$; it lies in the (A, B)-plane (where $X = Y = 0$), which is invariant since $k_6 = 0$. Equilibria along this